



Cite this: *Nanoscale*, 2023, **15**, 16959

Nanozymes with versatile redox capabilities inspired in metalloenzymes†

Rocío López-Domene, ^{a,b} Krishan Kumar,^a Jose Eduardo Barcelon, ^c Gabriela Guedes,^b Ana Beloqui^{*a,d} and Aitziber L. Cortajarena ^{*b,d}

Metalloenzymes represent exemplary systems in which an organic scaffold combines with a functional inorganic entity, resulting in excellent redox catalysts. Inspired by these natural hybrid biomolecules, biomolecular templates have garnered significant attention for the controlled synthesis of inorganic nanostructures. These nanostructures ultimately benefit from the protection and colloidal stabilization provided by the biomacromolecule. In this study, we have employed this strategy to prepare nanozymes with redox capabilities, utilizing the versatile catalytic profile of Pt-loaded nanomaterials. Thus, we have investigated protein-templated Pt-based nanoclusters of different sizes and compositions, which exhibit remarkable oxidase, catalase, and reductase-like activities. The interplay between the composition and catalytic activity highlighted the size of the nanocluster as the most prominent factor in determining the performance of the nanozymes. Additionally, we have demonstrated the use of protein-templated nanozymes as potential co-catalysts in combination with enzymes for coupled reactions, under both sequential and concurrent one-pot conditions. This study provides valuable insights into nanozyme design and its wide range of applications in the design of complex catalytic systems.

Received 14th July 2023,
Accepted 24th September 2023

DOI: 10.1039/d3nr03443g

rsc.li/nanoscale

1. Introduction

Enzymes represent excellent biomaterials capable of facilitating chemical reactions under mild conditions. However, these biocatalysts often suffer from limited stability and robustness, as well as narrow operating ranges concerning pH, temperature, and chemical environments. Consequently, the development of alternative catalysts to enzymes has gained considerable attention, leading to the emergence of nanozymes—synthetic nanomaterials that exhibit enzyme-like catalytic properties. To date, more than 540 distinct nanomaterials have been reported as nanozymes, with a majority incorporating metal components such as gold (Au), silver (Ag), palladium (Pd), copper (Cu), or platinum (Pt).^{1–6} These metals possess unique electronic and surface properties that confer high cata-

lytic efficiency for various chemical conversions. Among the breadth of nanomaterials exhibiting enzyme-like activities, such as nanoparticles, graphene, carbon nanotubes, metal-organic frameworks, and quantum dots, metal nanoclusters have emerged as particularly promising nanozymes. However, the catalytic potential of metal nanoclusters has not been fully explored, and their remarkable catalytic features remain largely unexploited in the field.^{7–10}

Metal nanoclusters (NCs) are small assemblies of a few to hundreds of metal atoms, known for their distinctive electronic and geometric characteristics. Consequently, they have attracted considerable interest in the fields of bioimaging, catalysis, lighting, and sensing.^{11–17} The reactivity and substrate interaction of metal clusters are strongly influenced by factors such as surface structure, size, and composition. However, it has been observed that as the size of the particles decreases, the surface free energy increases significantly. This phenomenon triggers the agglomeration of clusters into larger particles during the fabrication process, leading to significant alterations in their key properties. For this reason, strategies that pursue the colloidal stabilization of these nanomaterials are demanded.

Inspired by the composition and structure of metalloenzymes, protein-templated nanoclusters have emerged as a remarkable strategy for enhancing the stability, activity, and selectivity of the inorganic nanomaterial. This biomimetic approach involves utilizing a protein backbone to embrace the

^aPOLYMAT and Department of Applied Chemistry, Faculty of Chemistry, University of the Basque Country UPV/EHU, Paseo Manuel Lardizabal 3, Donostia-San Sebastián, 20018, Spain. E-mail: ana.beloqui@ehu.es

^bCenter for Cooperative Research in Biomaterials (CIC biomAGUNE), Basque Research and Technology Alliance (BRTA), Paseo de Miramón 194, Donostia-San Sebastián, 20014, Spain. E-mail: alcortajarena@cicbiomagune.es

^cDonostia International Physics Center, Paseo Manuel de Lardizabal 4, 20018 Donostia-San Sebastian, Spain

^dIKERBASQUE, Basque Foundation for Science, Plaza Euskadi 5, Bilbao, 48009, Spain

† Electronic supplementary information (ESI) available. See DOI: <https://doi.org/10.1039/d3nr03443g>



inorganic entity, creating a favorable environment that prevents the aggregation of nanoclusters. The protein template plays a major role in guiding the formation of metal clusters with distinct sizes, shapes, and configurations, resulting in metal-based catalytic sites that emulate the active sites found in natural enzymes. As a result, the protein-nanocluster hybrid provides both stability and a conducive microenvironment that protects the catalyst from deactivation.

Furthermore, the protein-nanocluster hybrid can be customized to address specific reactions. For example, Wang *et al.* synthesized bovine serum albumin (BSA)-protected gold nanoclusters (Au NCs) by the *in situ* reduction of gold ions using the tyrosine residues of the protein.¹⁸ This biohybrid showed peroxidase enzyme-like activity over a wide pH and temperature range. The redox capabilities of protein-NC hybrids have been demonstrated using BSA-AuNCs or lysozyme-PtNCs for the oxidation of 3,3',5,5'-tetramethylbenzidine (TMB), or ferritin-PtNCs for the disproportionation of hydrogen peroxide.^{19–21} However, most of the reported protein-templated NCs are prepared using proteins that have not been previously engineered. As a result, the allocation of the nanoclusters on the protein is not controlled, which can result in the aggregation of the biohybrids and/or limited control over the properties of the NC. In our recent works, we employed an engineered protein with a well-defined structure to direct the allocation of the nanoclusters and serve as a shield, protecting the metal clusters against aggregation, oxidation, and other detrimental effects.^{15,22,23} This approach permits the fabrication of an artificial catalytic pocket in which the nanoclusters act as the catalytic entity. By using a consensus tetratricopeptide repeat (CTPR) engineered protein template, we demonstrated the precise modulation of the catalytic properties, which depended not only on the nanocluster composition, but also on the chemical environment, including the coordinating residues to which the nanomaterial is exposed.¹⁵ Moreover, our approach offers several advantages, such as being environmentally friendly, simple, efficient, scalable, and avoids the need for hazardous reagents.

In this study, we have investigated the catalytic versatility of CTPR-templated nanozymes, with a specific focus on platinum (Pt)-loaded nanoclusters. These biohybrids, inspired by the structure and configuration of natural metalloenzymes, exhibit various redox performances, including oxidase, catalase, and reductase-like activities. We have examined the influence of NC size and composition on the catalytic oxidation of small molecules, the disproportionation of hydrogen peroxide, and the reduction of *p*-nitrophenol. Through this investigation, we have unveiled major connections between the features of the NCs and their catalytic performance in those reactions. Furthermore, we aimed to explore the potential interfacing of protein-templated nanozymes with natural enzymes in two-step reactions. By combining the best-performing biohybrid with *Candida antarctica* Lipase B (CALB) enzyme, we sought to broaden the application scope of the biohybrids while enhancing the overall process efficiency and streamlining.^{21,24} Specifically, we tested the reduction of *p*-nitrophenylbutyrate

(PNB) to *p*-aminophenol (PAP), using both a two-step sequential approach and a one-pot concurrent method, making use of the joint action of the engineered biohybrid and the CALB enzyme. This investigation highlights the compatibility and synergistic effects of protein-templated nanozymes with natural enzymes in complex reaction systems.

2. Results and discussion

2.1. Synthesis and characterization of protein-templated nanozymes

The synthesis of the biohybrids was carried out by leveraging the capability of engineered consensus tetratricopeptide repeat (CTPR) proteins to coordinate metals, accommodate, and eventually stabilize the nanoclusters within their designed binding pocket. Specifically, the CTPR mutant utilized in this work has been engineered with a metal-coordination module designed to accommodate the artificial catalytic site of the hybrid.¹⁷ This binding module consists of 16 histidines oriented towards the inner cavity with its concave face (Fig. 1A). The hybrid nanozyme is formed throughout the *in situ* assembly of the nanocluster in the proximity of the metal-binding module, as previously described.¹⁵ To achieve this, the desired amount of metal salt precursor, *e.g.*, K₂PtCl₄ for Pt nanozymes, was added to the CTPR solution at pH 10, followed by a 72 h incubation at 50 °C. We hypothesize that the functional groups, particularly the binding residues, of the protein can play an important role as “carriers” of the seeded metal cations under these conditions, facilitating the formation of hot spots that eventually lead to the synthesis of the nanoclusters.¹⁵ Subsequently, the metal cations were reduced *in situ* by the addition of sodium ascorbate as a reducing agent. Complete details on the nanocluster synthesis and purification procedures can be found in the ESI section,[†] providing a comprehensive overview of the methodology employed in this study.

In this study, our objective was to investigate the interplay between the size, composition, and redox capability of the biohybrids. To achieve this, we designed a series of Pt nanozymes with an increasing number of atoms, as well as a biohybrid which composition was doped with a second metal cation, namely Au. The synthesis process involved the seeding of CTPR proteins with increasing amounts of Pt^{II}, specifically 32, 64, 160, and 320 equivalents per protein. In parallel, Au/Pt bimetallic nanozymes were achieved by the coaddition of 320 and 32 equivalents of Pt and Au, respectively. Overall, a total of five Pt-based protein-templated nanozymes were successfully synthesized and characterized.

After the synthesis protocol, the protein-templated nanozymes were efficiently recovered with yields of 72 and 90% of the initial protein amount, for the lowest to the highest metal cation loads, respectively (Table S1[†]). The synthesis of the nanoclusters was validated by Transmission Electron Microscopy (TEM) imaging, and the size of the nanomaterials ranged from 1.29 to 1.95 nm, achieving larger nanomaterials for the largest Pt loads (Fig. 1A, Fig. S1 and Table S2[†]). Matrix-



2.2. Redox capability of the nanozymes

We recently explored the peroxidase-like activity of similar protein-templated nanozymes, which surpassed many of the Pt-based hybrid nanozymes reported so far. In this study, we explore the oxidation potential of a set of CTPR-templated nanozymes, loaded with different Pt contents in the absence of hydrogen peroxide, focusing first on oxidation reactions. In the first experiment, the oxygen consumption rate of Au₇Pt₇₄ nanozyme (from 1 to 10 μM) in the presence of pyrogallol (PG), as the substrate, was monitored *in situ* using an oxygen dipping probe (Fig. S4A†). Concentration-dependent oxygen consumption was observed. To analyze these results, we defined the oxygen consumption 50 (OC50) index as the time required for the nanozyme to reduce the oxygen content in the solution by half. Accordingly, OC50 values ranged from 40 to 140 s for nanozyme concentrations of 10 to 1 μM, respectively (Fig. S4B†). Fig. 2A clearly shows that the largest nanoclusters exhibited the fastest oxygen consumption rates under the same oxidation conditions when comparing the entire set of

nanozymes. As a general trend, the oxidation efficiency, as measured by OC50, could be correlated with the size of the nanocluster following an exponential trend, ranking the nanozymes from most to least active as follows: Au₇Pt₇₄ > Pt₄₆ > Pt₃₄ > Pt₁₆ > Pt₁₁ (Table S4 and Fig. S5†). Thus, while Au₇Pt₇₄ and Pt₄₆ nanozymes achieved a 50% reduction in oxygen concentration within 50 and 83 seconds, respectively, the Pt₁₁ nanozymes required more than 1400 seconds to reach similar oxidation yields. Furthermore, nanozymes with low Pt content, *i.e.*, Pt₁₁ and Pt₁₆, were unable to completely deplete the oxygen from the solution, indicating the limited catalytic potential of these hybrids. Conversely, the catalytic performance of Pt₄₆ and Au₇Pt₇₄ nanozymes did not exhibit significant differences despite the increase in the number of Pt atoms. This effect might be attributed to the exposed surface area, which might be, in this size range, the dominating factor in understanding the catalytic performance of the nanoclusters.

The catalytic performance of the nanozymes was ascertained by UV-Vis spectroscopy (Fig. S6†). The oxidation of PG could be traced by the increase of absorbance at 420 nm. The



Fig. 2 (A) Oxygen consumption measured for the set of nanozymes (reaction conditions: 5 μM of nanozymes, 3 mM of pyrogallol in 50 mM PB buffer at pH 7 and 25 °C). (B) Specific activity, in U mg⁻¹, measured for the set of nanozymes for the oxidation of pyrogallol (reaction conditions: 1 μM of nanozymes, 1 mM of pyrogallol in 50 mM PB buffer at pH 7 and 25 °C). The chemical structure of PG and the proposed structure for the oxidized PG are inserted. (C) Michaelis–Menten curves for Au₇Pt₇₄, Pt₄₆, and Pt₃₄ using 1 μM of nanozymes and 0–1 mM of pyrogallol in 50 mM PB buffer at pH 7. (D) Catalytic efficiency measured for the oxidation of TMB and ABTS reagents by Au₇Pt₇₄, Pt₄₆, and Pt₃₄.



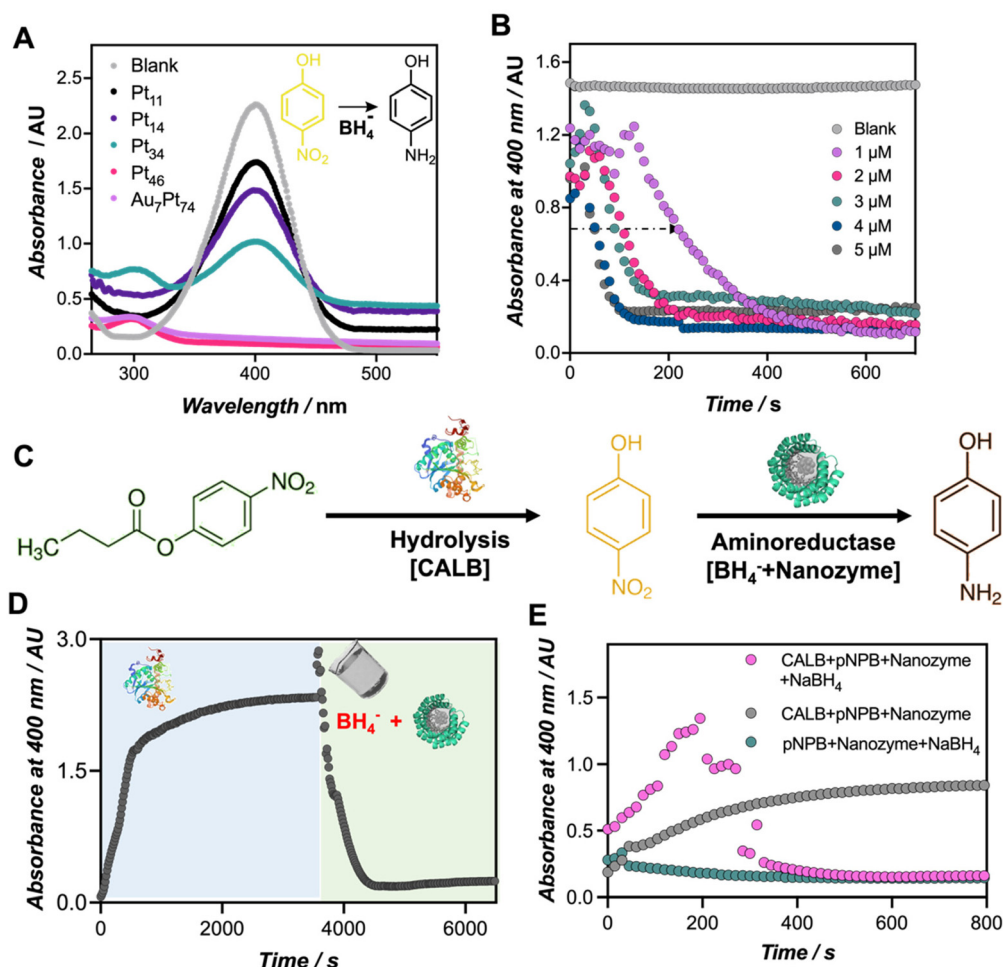
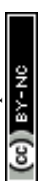


Fig. 4 Catalytic performance of nanozymes in the reduction of PNP to PAP and enzyme-coupled reactions. (A) Monitoring the reduction of PNP to PAP by UV-Vis for each of the nanozymes. (B) Reduction kinetics monitored at 400 nm at different concentrations of Au₇Pt₇₄ nanozyme. (C) Scheme of the sequential reaction carried out in this work. First, the PNB is hydrolyzed by CALB lipase and, in a second reaction, the released PNP is reduced by the joint action of NaBH₄ and the nanozyme. (D) Monitoring of the PNP absorbance after the sequential addition of the catalysts (CALB first—in blue —, and then the nanozymes—in green); (E) monitoring of the PNP absorbance along the one-pot concurrent reduction from PNB to PAP.

nanozymes holds great potential for sequential, as well as concurrent chemoenzymatic reactions. As a proof-of-concept, we assayed our best-performing biohybrid, Au₇Pt₇₄, in a sequential cascade reaction with CALB enzyme to convert *p*-nitrophenyl butyrate (PNB) to PAP (Fig. 4C). In the first step, we added the CALB enzyme to the PNB solution. Subsequently, the nanozyme hybrid was added together with the NaBH₄ hydride donor. We performed the reaction in a 96-well plate, and the formation and conversion of PNP were monitored at 400 nm (Fig. 4D). Under the applied conditions, CALB catalyzed the complete hydrolysis of PNB in less than 30 min, as indicated by the saturation of the signal at 400 nm. In the second step, the co-addition of the nanozyme and NaBH₄ triggered a sudden increase in pH, leading to a rise in the extinction coefficient of the *p*-nitrophenolate chromophore (Fig. S13†). Subsequently, this co-addition of the nanozyme and NaBH₄ resulted in the disappearance of the signal corresponding to PNP and the emergence of a band at 300 nm, likely indicating

the formation of PAP, and confirming the occurrence of this second reduction reaction (Fig. S14†).³³

Motivated by these results, we proceeded to perform the same reaction under one-pot conditions, which would provide insights into the compatibility of the biohybrids with functional proteins such as enzymes. For this purpose, we prepared a cocktail comprising both natural (CALB) and artificial (Au₇Pt₇₄) enzymes along with the hydride donor, NaBH₄. To monitor this reaction by UV-Vis spectroscopy, two reaction controls were tested. As depicted in Fig. 4E, in the absence of the CALB enzyme, no PNP conversion was detected (green dots in Fig. 4E), emphasizing the role of the *p*-nitrophenolate species in the reduction mechanism to PAP.^{34,35} Additionally, we observed that the presence of a hydride donor, NaBH₄, is necessary to initiate the reduction reaction (grey dots in Fig. 4E), which was also accompanied by the rise of the band at 300 nm corresponding to PAP (Fig. S15†). Finally, the co-addition of all the reactants led to the release of PNP, which,



at a given concentration, is likely further converted *in situ* to PAP, evidenced by a sudden drop of the absorbance at 400 nm. Therefore, we have successfully demonstrated the efficient concurrence of two catalytic transformations driven by a natural enzyme and a nanozyme within the same reaction environment.

3. Conclusions

This study reveals compelling conclusions on the design and versatility of Pt nanoclusters stabilized by CTPR protein. It has been demonstrated that the *in situ* synthesis procedure can be controlled for the achievement of nanoclusters comprising 11 to 74 Pt atoms. Interestingly, the addition of a small fraction of gold atoms into the synthesis, *i.e.*, 10% (n/n), triggers up to a 38% increase in the incorporation of Pt into the nanomaterial. However, the role of the gold atoms appears to be merely structural. The kinetic profile of the metal nanoclusters fits well with the Michaelis–Menten model, indicating the successful development of robust nanozymes with redox capabilities. Moreover, there is an exponential relationship between the dimensions and the catalytic performance of the hybrids. While the smallest hybrids, *i.e.*, Pt₁₁, Pt₁₆, and Pt₃₄, exhibit limited redox catalysis, Pt₄₆, and Au₇Pt₇₄, with similar catalytic performance, exhibit oxygen consumption rates up to 200 times higher. Moreover, an insightful structural and functional characterization of the hybrids reveals that the catalytic performance is not solely influenced by the size; rather, parameters such as surface area and the oxidation state of the Pt atoms must also be taken into consideration.

We have explored the application of protein-templated nanozymes in sequential and concurrent chemoenzymatic reactions. Our focus was centered on assessing the performance of the most effective biohybrid in catalyzing a sequential cascade reaction coupled to CALB enzyme, resulting in the successful conversion of PNB into PAP. This demonstrates the capability of interfacing protein-templated nanozymes with natural enzymes, which broadens the applicability of these nanozymes. Thus, the demonstrated catalytic versatility, together with the possibility to use them together with other enzymes, underline the role of CTPR-templated Pt nanoclusters as promising catalysts in various technological fields, such as environmental remediation, biosensing, biomedicine, and energy conversion among others.

Conflicts of interest

There are not conflicts to declare.

Acknowledgements

A. L. C. acknowledges support by the Agencia Estatal de Investigación Grant PID2019-111649RB-I00 and PID2022-137977OB-I00 funded by MCIN/AEI/10.13039/501100011033

and Grant PDC2021-120957-I00 funded by MCIN/AEI/10.13039/501100011033 and by the “European Union NextGenerationEU/PRTR”. This work was performed under the Maria de Maeztu Units of Excellence Program from Q5 the Spanish State Research Agency grant no. MDM-2017-0720. A. B. gratefully acknowledges the financial support from the Spanish Research Agency (AEI) for the financial support (PID2022-142128NB-I00 funded by MCIN/AEI/10.13039/501100011033 and by the “European Union NextGenerationEU/PRTR”; RYC2018-025923-I from RyC program – MCIN/AEI/10.13039/501100011033 and FSE “invierte en tu futuro”), BBVA Foundation – IN[21]_CBB_QUI_0086, and UPV/EHU – GIU21-033. K.K. thanks JdC Grant FJC2021-047607-I funded by MCIN/AEI/10.13039/501100011033. We thank Fernando López-Gallego for support with the oxygen consumption measurements.

References

- 1 N. Pajoohehpour, M. Rezaei, A. Hajian, A. Afkhami, M. Sillanpää, F. Arduini and H. Bagheri, *Sens. Actuators, B*, 2018, **275**, 180–189.
- 2 J. Xie, Y. Zheng and J. Y. Ying, *J. Am. Chem. Soc.*, 2009, **131**, 888–889.
- 3 B. Jiang and M. Liang, *Chin. J. Chem.*, 2021, **39**, 174–180.
- 4 Y. Jiang, Z. Ding, M. Gao, C. Chen, P. Ni, C. Zhang, B. Wang, G. Duan and Y. Lu, *Chin. J. Chem.*, 2021, **39**, 3369–3374.
- 5 H. Wei and E. Wang, *Chem. Soc. Rev.*, 2013, **42**, 6060–6093.
- 6 J. Wu, X. Wang, Q. Wang, Z. Lou, S. Li, Y. Zhu, L. Qin and H. Wei, *Chem. Soc. Rev.*, 2019, **48**, 1004–1076.
- 7 L. Chen, T. Hou, Y. Tan, C. Guo, B. Wang, L. Ge and F. Li, *ACS Sustainable Chem. Eng.*, 2022, **10**, 2750–2760.
- 8 H. Wang, P. Li, D. Yu, Y. Zhang, Z. Wang, C. Liu, H. Qiu, Z. Liu, J. Ren and X. Qu, *Nano Lett.*, 2018, **18**, 3344–3351.
- 9 X. Niu, X. Li, Z. Lyu, J. Pan, S. Ding, X. Ruan, W. Zhu, D. Du and Y. Lin, *Chem. Commun.*, 2020, **56**, 11338–11353.
- 10 L. Zhao, Z. Wu, G. Liu, H. Lu, Y. Gao, F. Liu, C. Wang, J. Cui and G. Lu, *J. Mater. Chem. B*, 2019, **7**, 7042–7051.
- 11 W. Huang, X. Ma, O. Sato and D. Wu, *Chem. Soc. Rev.*, 2021, **50**, 3176–3191.
- 12 S. I. Tanaka, J. Miyazaki, D. K. Tiwari, T. Jin and Y. Inouye, *Angew. Chem., Int. Ed.*, 2011, **50**, 431–435.
- 13 F. Molaabasi, M. Sarparast, M. Shamsipur, L. Irannejad, A. A. M. Movahedi, A. Ravandi, B. H. Verdom and R. Ghazfar, *Sci. Rep.*, 2018, **8**, 14507.
- 14 X. Meng, I. Zare, X. Yan and K. Fan, *Wiley Interdiscip. Rev. Nanomed. Nanobiotechnol.*, 2020, **12**, e1602.
- 15 R. L. Domene, S. V. Díaz, E. Modin, A. Belouqui and A. L. Cortajarena, *Adv. Funct. Mater.*, 2023, 2301131.
- 16 N. Goswami, K. Zhenga and J. Xie, *Nanoscale*, 2014, **6**, 13328.
- 17 A. Aires, V. F. Luna, J. F. Cestau, R. D. Costa and A. L. Cortajarena, *Nano Lett.*, 2020, **20**, 2710–2716.



- 18 X. X. Wang, Q. Wu, Z. Shan and Q. M. Huang, *Biosens. Bioelectron.*, 2011, **26**, 3614–3619.
- 19 G. L. Wang, L. Y. Jin, Y. M. Dong, X. M. Wu and Z. J. Li, *Biosens. Bioelectron.*, 2015, **64**, 523–529.
- 20 C. J. Yu, T. H. Chen, J. Y. Jiang and W. L. Tseng, *Nanoscale*, 2014, **6**, 9618–9624.
- 21 J. Fan, J. J. Yin, B. Ning, X. Wu, Y. Hu, M. Ferrari, G. J. Anderson, J. Wei, Y. Zhao and G. Nie, *Biomaterials*, 2011, **32**, 1611–1618.
- 22 A. Aires, A. Sousaraei, M. Möller, J. C. Gonzalez and A. L. Cortajarena, *Nano Lett.*, 2021, **21**, 9347–9353.
- 23 A. Aires, I. Llarena, M. Moller, J. C. Smirnov, J. C. Gonzalez and A. L. Cortajarena, *Angew. Chem., Int. Ed.*, 2019, **58**, 6214–6219.
- 24 N. L. Garcia, A. J. Alesanco, A. V. Campoy, O. Abian and J. M. Palomo, *ACS Appl. Mater. Interfaces*, 2021, **13**, 5111–5124.
- 25 D. Xu, L. Wu, H. Yao and L. Zhao, *Small*, 2022, **37**, 2203400.
- 26 J. Li, W. Liu, X. Wu and X. Gao, *Biomaterials*, 2015, **48**, 37–44.
- 27 S. Shirin, S. Roy, A. Rao and P. P. Pillai, *J. Phys. Chem. C*, 2020, **124**, 19157–19165.
- 28 S. Roy, A. Rao, G. Devatha and P. P. Pillai, *ACS Catal.*, 2017, **7**, 7141–7145.
- 29 N. L. Garcia, E. P. Urriolabeitia and J. M. Palomo, *ACS Appl. Nano Mater.*, 2023, **6**, 704–713.
- 30 S. Pandey and S. B. Mishra, *Carbohydr. Polym.*, 2014, **113**, 525–531.
- 31 T. A. Thiel, X. Zhang, B. Radhakrishnan, R. van de Krol, F. F. Abdi, M. Schroeter, R. Schomäcker and M. Schwarze, *RSC Adv.*, 2022, **12**, 30860–30870.
- 32 R. D. Neal, R. A. Hughes, P. Sapkota, S. Ptasinska and S. Neretina, *ACS Catal.*, 2020, **10**, 10040–10050.
- 33 J. Strachan, C. Barnett, A. F. Masters and T. Maschmeyer, *ACS Catal.*, 2020, **10**, 5516–5521.
- 34 R. Grzeschik, D. Schäfer, T. Holtum, S. Küpper, A. Hoffmann and S. Schlücker, *J. Phys. Chem. C*, 2020, **124**, 2939–2944.
- 35 C. Kästner and A. F. Thünemann, *Langmuir*, 2016, **32**, 7383–7391.

